Radiation-induced intrinsic defects in TeO_2

1990 J. Phys.: Condens. Matter 2 4325

(http://iopscience.iop.org/0953-8984/2/19/002)

J. Phys.: Condens. Matter 2 (1990) 4325–4339. Printed in the UK

Radiation-induced intrinsic defects in TeO_2

G Corradi†‖, A Watterich‡, I Földvári‡, R Voszka‡, J R Niklas†, J-M Spaeth†, O R Gilliam§ and L A Kappers§

† Universität Paderborn, Fachbereich Physik, Warburger Strasse 100A, D-4790 Paderborn, Federal Republic of Germany

‡ Research Laboratory for Crystal Physics of the Hungarian Academy of Sciences, PO Box 132, H-1502 Budapest, Hungary

§ Department of Physics and Institute of Materials Science, University of Connecticut, Storrs, CT 06269, USA

Received 5 December 1989

Abstract. In undoped paratellurite (α-TeO_2) electron-irradiated near room temperature, in addition to the $V_O^{\bullet}$ centre described earlier, two further intrinsic, strongly anisotropic radiation defects have been characterised using ESR and ENDOR spectroscopy. The first new centre is assumed to be an aggregate of two oxygen vacancies with a net positive charge and denoted as $(V_O)_2^{\bullet}$. According to this model the unpaired spin is mainly distributed along a quasilinear Te–O–Te–O–Te chain with the vacancies in short-bond positions relative to the central tellurium. Based on apparent analogies a similar delocalisation is suggested for the $V_O^{\bullet}$ centre as well. For the second new centre the 'small peroxy radical' model originally proposed for SiO_2 by Edwards and Fowler has been adapted, where an oxygen interstitial is trapped next to a lattice oxygen, the latter also maintaining its bonds to both Te neighbours (Te–O_2–Te).

1. Introduction

Defects produced by electron irradiation in undoped paratellurite (α-TeO_2), an excellent acousto-optic material have recently been investigated by Watterich *et al* (1985) using ESR. A most prominent intrinsic radiation defect, which is stable at room temperature (RT), has been characterised at 92 K as an oxygen vacancy with a net positive charge, i.e. a $V_O^{\bullet}$ centre in the Kröger–Vink (1959) notation (Watterich *et al* 1985). As supported also by a molecular cluster calculation (Corradi *et al* 1987) the unpaired spin in the $V_O^{\bullet}$ centre is primarily concentrated on the short-bond Te neighbour of the vacancy and has appreciable superhyperfine (SHF) interactions with a number of other unidentified Te neighbours. These characteristics are intermediate between those of the strongly localised E_1' centre in α-SiO_2 and the more diffuse F^+ centre in the alkaline earth oxides. The $V_O^{\bullet}$ centre was also found to form close associates with impurities (Watterich *et al* 1986a, b).

In the present work a low temperature ESR and electron nuclear double resonance (ENDOR) study of undoped TeO_2 irradiated with massive electron doses near RT has been

‖ Permanent address: Research Laboratory for Crystal Physics of the Hungarian Academy of Sciences, PO Box 132, H-1502 Budapest, Hungary.

0953-8984/90/194325 + 15 $03.50

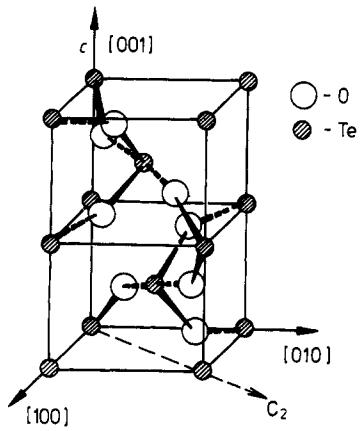

Figure 1. Primitive cell of paratellurite. One of the C_2 symmetry axes is shown. Short bonds are indicated by heavy full lines and long bonds by heavy broken lines.

carried out. In addition to known centres two further basic intrinsic defects, stable above RT but observable only at low temperatures, have been found and characterised. The results also lead to a better understanding of the $V_O^{\cdot}$ centre and the radiation process.

2. Crystal structure

In the paratellurite phase TeO_2 has a distorted rutile structure (see figure 1) with the tetragonal space group D_4^4 and lattice constants $a = 4.8122$ Å and $c = 7.6157$ Å (Lindquist 1968). Each tellurium is situated on a C_2 symmetry axis of [110] type, is slightly displaced along this direction from the rutile-like position and has a fourfold oxygen coordination with two short-bond (1.902 Å) and two long-bond (2.068 Å) oxygen neighbours, all within the same {110} type half-space (see figure 1). The oxygens occupy positions with no symmetry (C_1). Accordingly, four and eight orientationally (magnetically) inequivalent Te and O sites can be distinguished, respectively.

3. Experimental methods

Single crystals of pure TeO_2 (<5 ppm) were grown by a balance-controlled Czochralski technique (Schmidt and Voszka 1981). Samples of the sizes $9 \times 3.5 \times 2$ mm with the long edge along [110] or [100] were subjected in the typical cases to electron irradiation from a Van de Graaff accelerator operated at 1.65 MV with sample nominal current densities of 6 μA cm^{-2} for 10 h on both sides. Some crystals subjected to smaller doses were used for comparison. No cooling was applied; accordingly, the sample holder reached a temperature of $\simeq$60 °C during irradiation. The originally transparent samples became black and non-transparent even in the infrared with absorption extending beyond 1000 nm.

Most ESR and stationary ENDOR experiments were performed with a custom built computer-controlled X-band spectrometer. The sample temperature could be varied between 4 K and 300 K; the ENDOR frequency could be varied in the range between 0.5 and 160 MHz. The ESR and ENDOR line positions were determined by using digital filtering, deconvolution algorithms and a special peak search algorithm (Niklas 1983).

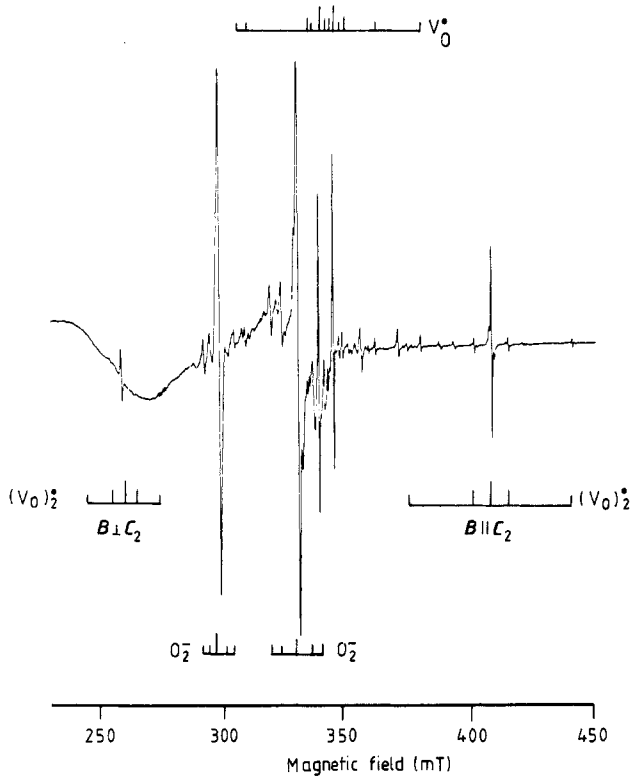

Figure 2. ESR spectrum at $T = 8$ K of undoped TeO_2 irradiated with 1.65 MeV electrons near RT. The magnetic field orientation is $\boldsymbol{B} \parallel [110]$. The lines of three basic radiation defects each having two magnetically inequivalent orientations for $\boldsymbol{B} \parallel [110]$ are indicated. The broad line near 250 mT is due to the resonator.

Some RT and 78 K ESR measurements and optical characterisation were carried out using a Varian E-3 X-band ESR and a Cary 14 R optical spectrometer, respectively.

4. Experimental results

4.1. General features

RT electron irradiation produces a number of paramagnetic defects in undoped TeO_2. With ESR at low temperatures, in addition to substantial concentrations of the $V_O^{\bullet}$ centre and trace amounts of the initially present Pt^{3+} centres (Watterich *et al* 1987a), at least four unknown radiation defects have been detected. Only two of them had large enough concentrations for a detailed study; these will be described in this paper. No decrease of the ESR intensities could be observed after several months of RT storage of the samples in the dark, or as a result of handling them under normal illumination conditions. For smaller radiation doses the relative intensities of both important new centres are found to decrease with respect to the $V_O^{\bullet}$ centres.

The ESR spectrum for the magnetic field $\boldsymbol{B}$ parallel to [110] is shown in figure 2. For both new centres the pairs of satellites can be attributed to super- or hyperfine (SHF or

HF) interaction with the magnetic ^{125}Te species ($I = \frac{1}{2}$, natural abundance 6.99%) which is similar in the case of the $V_O^{\cdot}$ centre. ^{123}Te satellites are not seen due to the low abundance of this isotope (0.9%).

4.2. *The $(V_O)_2^{\cdot}$ centre*

The first new centre has sharp ESR lines and a HF splitting of $\leqslant$70 mT, nearly as large as that of the $V_O^{\cdot}$ centre (see figure 2). For temperatures higher than $\simeq$50 K the intensity of the spectrum strongly decreases, but the lines reappear upon recooling. For temperatures close to 4 K the centre shows saturation effects, though to a lesser extent than the $V_O^{\cdot}$ centre. The large doublet splitting is evidently due to strong HF interaction with a single, central Te nucleus which we denote Te_c. The other ^{125}Te satellites with weaker coupling appear to have doubled relative intensities (7% instead of 3.5% for each line) compared to the respective central lines and must be attributed to pairs of Te sites. Two pairs of such satellites, corresponding to two pairs of Te neighbours are resolved in the ESR spectrum.

The angular dependence of the ESR spectrum is shown in figure 3. The most striking features are C_2 centre symmetry and the large correlated anisotropies of the **g** tensor and of the strong Te HF interaction. In fact, the eigenvectors of the respective tensors **g** and $\mathbf{A}_c$ are the same within experimental error. All results are consistent with $S = \frac{1}{2}$. The values of the ESR parameters are given in table 1. The anisotropies of the SHF interactions of the first two Te shells were too small to be detected.

Using ENDOR the ^{125}Te SHF constants for ten more Te shells could be determined, each containing a pair of Te nuclei related by C_2 symmetry. Thus, magnetic interactions with altogether 25 Te nuclei have been determined. The ENDOR spectrum for $\boldsymbol{B} \parallel \boldsymbol{C}_2$ is shown in figure 4; an example of the angular dependence is given in figure 5. The data are summarised in table 2. The interactions are given in terms of the isotropic (a) and anisotropic (b, b') SHF constants and Euler angles, the principal values being $A_x = a - b + b'$, $A_y = a - b - b'$ and $A_z = a + 2b$. For more details on ENDOR see, e.g., Seidel (1961) and Spaeth (1988).

4.3. *The peroxy radical*

The second new centre appears to have the largest concentration, broader ESR lines but smaller splittings (see figure 2). Its ESR spectrum is broadened for $T \geqslant 90$ K.

As seen from the angular dependence (see figure 6) this ESR spectrum is due to a centre with C_1 symmetry and $S = \frac{1}{2}$. The **g** tensor and SHF data for three Te nuclei are given in table 3. Three more shells (distant) yield weak ENDOR signals which have not been investigated in detail.

5. Discussion

Both new defects are markedly different from the impurity-related ones known of so far in TeO_2 (Watterich *et al* 1986a, b, 1987a, b) and, what is more important, they are produced in non-saturating concentrations larger by several orders of magnitude than, e.g., those of Pt^{3+} centres. Therefore we ascribe both new spectra to intrinsic defects.

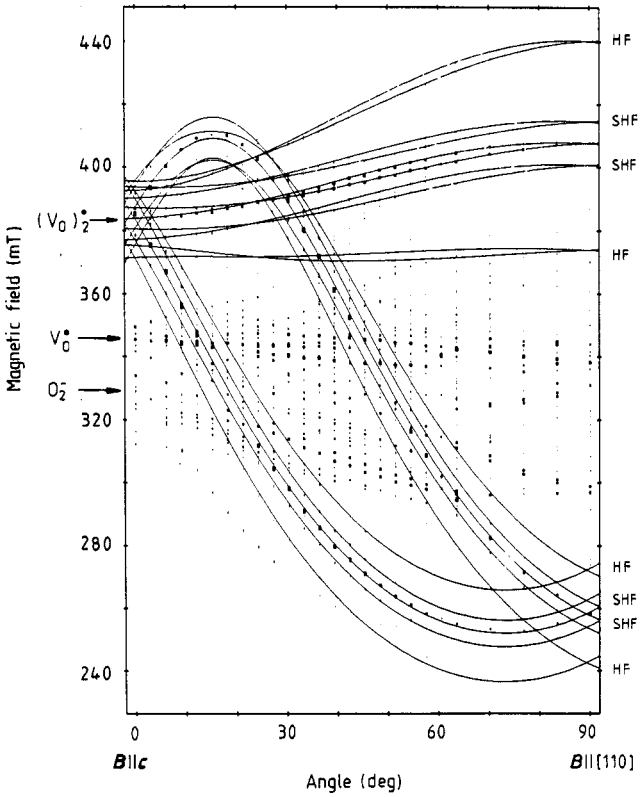

Figure 3. Angular dependence of ESR line positions at 8 K in electron-irradiated TeO_2. Dot sizes indicate experimental line intensities. The curves indicate $(V_O)_2^{\bullet}$ line positions simulated using data in table 1. In addition to the non-magnetic central line the pair of HF satellites and the first pair of SHF satellites due to the ^{125}Te isotope are shown. The exact symmetry of this centre is C_2, the small splitting of the high-field branch is due to a small 'misalignment' of the crystal. The other dots are due to $V_O^{\bullet}$, peroxy and other radiation centres (some off-scale lines of the peroxy centre are not represented here).

5.1. The $(V_O)_2^{\bullet}$ centre

A basic property of the first new centre is the observed C_2 symmetry. The outstanding eigenvalue $A_x^{(c)} = 1718$ MHz for Te_C ($A_x^{(c)}$ corresponds to the C_2 axis and contains a large isotropic part $a_c = 1053$ MHz) can only be understood by assuming a symmetric (Γ_1) ground state. Accordingly, this state should mainly consist of s and p_x orbitals on Te_c.

The following structural models may be considered:

(i) a self-trapped electron (or hole) on a tellurium atom of the lattice;

(ii) two oxygen vacancies situated in short-bond (SB) neighbour positions of Te_C with a net positive charge, i.e., a $(V_O)_2^{\bullet}$ centre in SB configuration; and

(iii) a $(V_O)_2^{\bullet}$ centre in long-bond (LB) configuration.

Model (i) is unlikely because of the stability of the centre even above RT and because of its huge anisotropy, by far exceeding that of the $V_O^{\bullet}$ centre. Another argument against

Table 1. ESR parameters of $(V_O)_2^+$ centres compared to those of V_O^+ centres in TeO_2. The principal values (bold numbers) and eigenvectors for the **g** tensors and the ^{125}Te **A** HF tensors (the eigenvectors of both tensors coincide for $(V_O)_2^+$) and the nearly isotropic ^{125}Te SHF splittings measured at $\boldsymbol{B} \parallel \boldsymbol{c}$ for all four Te nuclei having an existing or disrupted oxygen bridge to the central Te. All HF and SHF tensor values are in MHz, direction cosines are given with respect to the crystallographic axes. The data for V_O^+ are taken from Watterich *et al* (1985), but new assignments for nuclei 1–4 are proposed. The centre orientations correspond to those of figures 7(*a*) and (*b*). The estimated errors are 0.001 for *g*-values, 4% for *A*-values and 0.5° for the directions.

Centre		*x*	*y*	*z*	^{125}Te ligands on the other side of LB oxygen	^{125}Te ligands on the other side of SB oxygen
$(V_O)_2^+$	**g**	**1.629**	**1.618**	**2.792**		
	$\mathbf{A}_c$	**1718**	**217**	**1226**		
		0.707	−0.196	0.679	$A_I \simeq 360$	$A_{II} \simeq 30$
		0.707	0.196	−0.679		(near vacancy)
		0	0.961	0.277		
V_O^+	**g**	**1.9705**	**1.9358**	**2.0105**		
		0.508	−0.590	0.628		
		0.728	−0.096	−0.679		
		0.461	0.802	0.381	$A_1 \simeq 237$	$A_3 \simeq 132$
	$\mathbf{A}_s$	**2328**	**1785**	**1599**		(near oxygen)
		0.614	−0.383	0.690	$A_2 \simeq 218$	$A_4 \simeq 36$
		0.750	0.012	−0.661		(near vacancy)
		0.245	0.924	0.295		

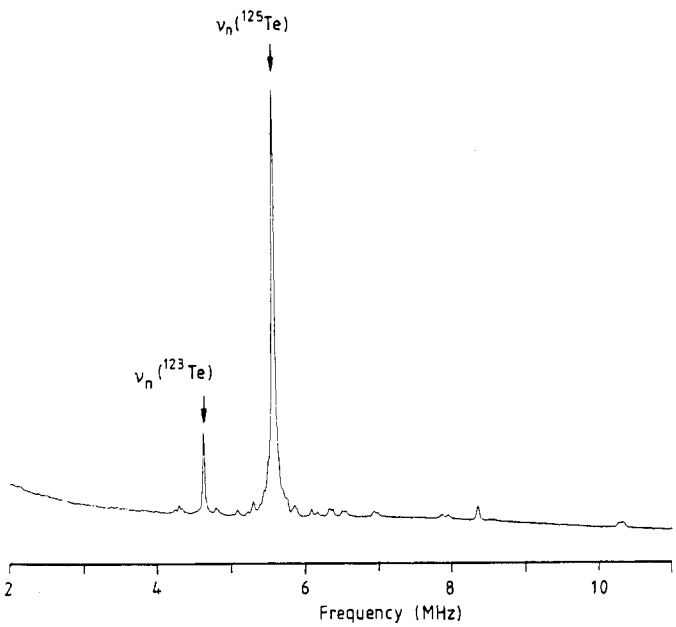

Figure 4. ENDOR spectrum at $T = 8$ K of the $(V_O)_2^+$ centre for the high-field central ESR line at $\boldsymbol{B} \parallel \boldsymbol{C}_2$. The intense peaks are due to distant ^{125}Te and ^{123}Te nuclei (ν_n denotes the nuclear Larmor frequencies) and the small lines to ^{125}Te nuclei in shells III–XII.

Table 2. ^{125}Te SHF parameters (in MHz) of $(V_O)_2^{\cdot}$ centres in TeO_2 derived with ENDOR. The shells are numbered in order of decreasing SHF splitting at $\boldsymbol{B} \parallel \boldsymbol{c}$. Assignments are given in a quasi-rutile frame of reference in units $\sim a/2$, $\sim a/2$ and $c/4$. Distances r from the central Te are in Å. The orientations of the principal axes x, y, z for each shell are given with respect to a crystal system $x_{cr} \parallel [110]$, $y_{cr} \parallel [001]$, $z_{cr} \parallel [1\bar{1}0]$ by the Euler angles $\theta = \angle(z, z_{cr})$, $\psi = \angle(x, s)$, $\varphi = \angle(s, x_{cr})$, where s is the intersection of planes xy and $x_{cr}y_{cr}$. The positive direction of s is fixed by the requirement that z, z_{cr} and s should form a right-handed system, and the signs of ψ and φ are positive for rotation from x to y. Estimated errors are 0.05 MHz and 2°

Te shell	III	IV	V	VI	VII	VIII	IX	X	XI	XII
a	10.7	5.64	2.28	4.45	1.44	2.40	2.3	1.0	0.24	0.92
b	3.3	−0.30	1.66	0.67	0.71	0.56	1.6	0.2	0.27	0.53
b'	2.1	<0.01	1.27	0.44	1.97	0.32	1.5	0.1	0.62	~0
θ	137°	105°	109°	54°	105°	172°	134°	~140°	68°	61°
ψ	−1°	—	−2°	123°	167°	90°	74°	~30°	1°	—
φ	−1°	44°	−7°	120°	141°	0°	131°	~80°	−4°	89°
Assignments	$[\bar{1}11]$	$[\bar{1}\bar{1}1]$	[002]	[022]	$[0\bar{2}2]$	$[2\bar{2}0]$	[202]	$[0\bar{2}0]$	$[1\bar{1}3]$	[200]
r	4.07	4.07	3.83	5.93	6.35	6.81	5.93	4.81	6.75	4.81

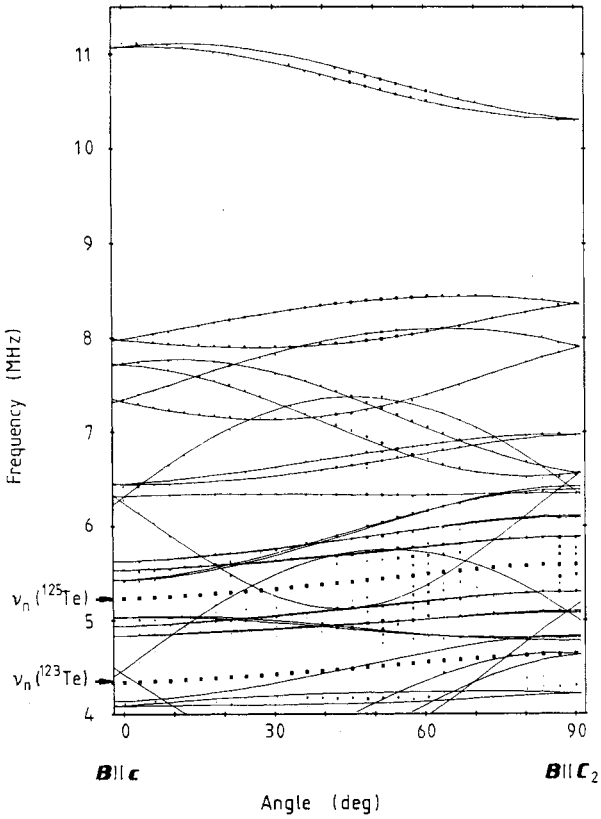

Figure 5. Angular dependence of the ENDOR line positions of the $(V_O)_2^{\cdot\cdot}$ centre for rotation of the magnetic field from the c axis to the C_2 axis of the centre. Dots represent experimental values, the curves are calculated using the data in table 2 for Te shells III–XII and ν_n are nuclear Larmor frequencies.

self-trapping and in favour of a divacancy model is the close relationship between the new centre and the $V_O^{\cdot\cdot}$ centre to be discussed in this section.

The eigenvectors of the largest g-values (g_z) for both the centre considered and the $V_O^{\cdot\cdot}$ centre are closely parallel to an O_{LB}–O_{LB} line (direction cosines 0.688, −0.688 and 0.231) connecting both long-bond oxygen neighbours of Te in perfect TeO_2 (3° and 9° deviation, respectively, see table 1). For the new centre this can be achieved by choosing from only 2 out of the 4 centre orientations; for the $V_O^{\cdot\cdot}$ centre the corresponding choice was made earlier on the basis of the molecular cluster model of Corradi *et al* (1987). Once these choices are made, one of the eigenvectors of the strong HF interaction for each centre also coincides with the same O_{LB}–O_{LB} direction (3° and 4° deviation, respectively; compare eigenvectors in column z of table 1). Moreover, the corresponding HF eigenvalues for z are rather close to each other (1226 and 1599 MHz), closer than the largest ones for each centre. These properties indicate that in the new centre, compared to $V_O^{\cdot\cdot}$, there should be little change on the LB neighbour sites of Te_c; however, a second oxygen vacancy on the other SB site, restoring C_2 symmetry for the new centre, should be present.

Thus we arrived at the SB configuration of the $(V_O)_2^{\cdot\cdot}$ model depicted in figure 7(*a*). Now we show that this model, in contrast to the LB configuration, is able to account for the observed features of the new centre.

According to the SB configuration model the core of the centre is a slightly bent –O–Te_c–O– chain flanked by two oxygen vacancies on one side and structural voids on the

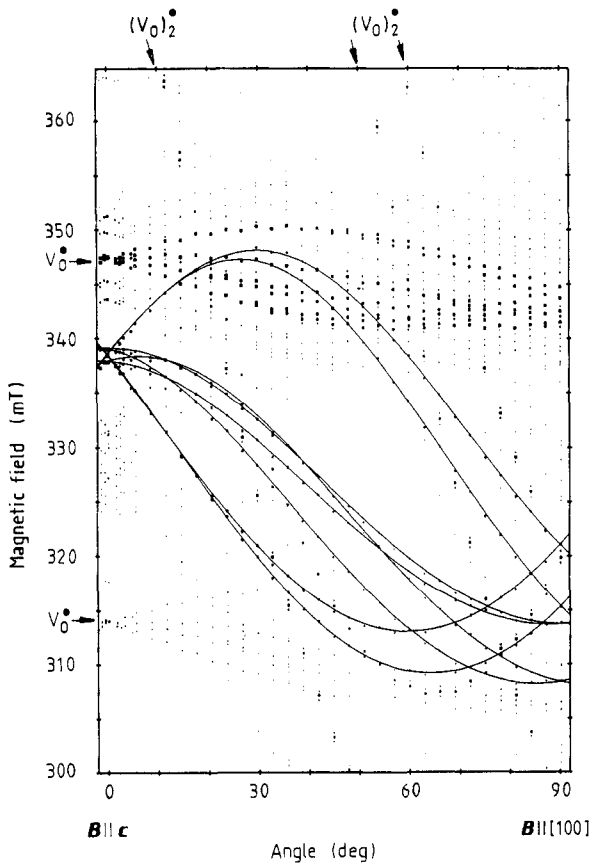

Figure 6. Angular dependence of ESR line positions at 13 K in electron-irradiated TeO_2. Only central line positions of the peroxy centre are simulated using data in table 3. The presence of eight lines is due to C_1 symmetry and a small 'misalignment' of the crystal from the indicated orientations. Prominent lines of other centres are indicated.

Table 3. ESR parameters of the peroxy radical in TeO_2. Principal values and eigenvectors (with respect to the crystallographic axes) for the **g** tensor and also for the ^{125}Te SHF tensors (in MHz) of the three Te neighbours shown in figure 8 are given. For errors see table 1.

	x	*y*	*z*
g	**2.092**	**1.929**	**2.311**
	0.514	0.552	−0.656
	−0.657	−0.239	−0.715
	−0.552	0.799	0.240
$\mathbf{A}_1$	**606**	**~88**	**881**
	0.469	0.303	−0.829
	−0.295	0.939	0.176
	0.832	0.162	0.530
$\mathbf{A}_2$	**222**	**140**	**955**
	0.388	−0.811	−0.438
	0.922	0.346	0.176
	0.009	−0.472	0.882
$\mathbf{A}_3$	**87**	**67**	**87**
		0.297	
		−0.061	
		0.953	

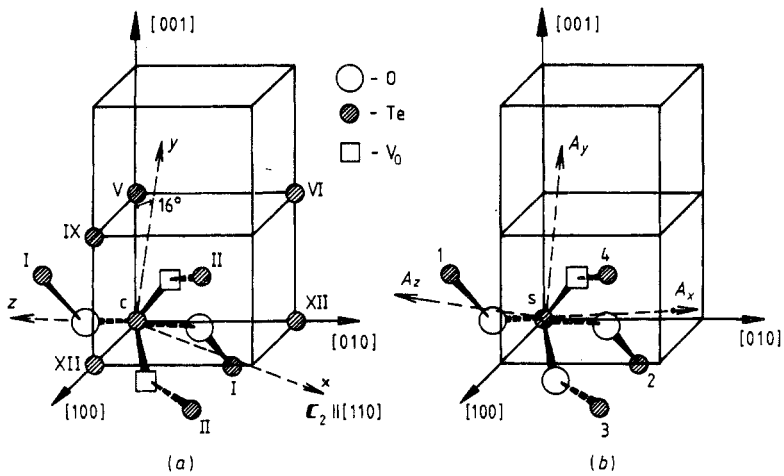

Figure 7. Model of the $(V_O)_2^{\cdot}$ centre in TeO_2 (*a*) compared with an extension of the model of the $V_O^{\cdot}$ centre originally proposed by Watterich *et al* (1985) (*b*) c and s indicate the Te nuclei where the unpaired electron spin is primarily concentrated; *x*, *y*, *z* for $(V_O)_2^{\cdot}$ are the common principal axes of the **g** and HF tensors. The principal HF axes for $V_O^{\cdot}$ are also indicated. The assigned Te shells given in table 1 and some of those given in table 2 are also shown. Except for oxygens bound to the central Te, nuclei with unknown SHF interactions are omitted. The choice between assignments 1 and 2 for the $V_O^{\cdot}$ centre is arbitrary.

other, the nearest other neighbours of Te_c being eight Te sites at distances 3.74 or 4.07 Å in the perfect crystal. The chain is roughly along a body diagonal of an otherwise empty half primitive cell formed by the eight Te sites (see figure 1). The large bonding angle at Te_c (168.5° without relaxation) explains the nearly axial and strongly anisotropic character of the **g** tensor. In fact, a nearly linear –O–Te–O– chain along *z* may have a nearly degenerate ground state leading to a large Δg_z. Relaxation may be decisive in reinforcing this character. For the $V_O^{\cdot}$ centre such an 'inward' relaxation of the central Te, labelled s in figure 7(*b*), (into the plane of its three oxygen neighbours) was in fact found (Corradi *et al* 1987). As supported also by the results of Strömberg *et al* (1985), tellurium left with only three oxygen neighbours tends to shorten its internuclear distances down to at least 1.9 Å, thereby appreciably changing the bonding angles which appear to be 'soft' coordinates compared to internuclear distances. The Te–O internuclear distances in the free TeO_2 molecule have been measured to be only 1.83 Å (Muenow *et al* 1969). The distance between oxygens in a LB-LB O–Te–O chain in perfect TeO_2 is 4.15 Å; accordingly, almost complete linearisation of the chain in the model may be expected. Apparently there is some tension in the full Te–O–Te_c–O–Te chain spanning it closer to the mentioned body diagonal. This may easily explain the observed 3° tilt of the g_z direction from the unrelaxed O_{LB}–O_{LB} direction towards the body diagonal. It should be noted that the average *g* shift of the new centre is positive ($\Delta\bar{g}$ = 0.011 in contrast to the $V_O^{\cdot}$ centre where $\Delta\bar{g} = -0.030$). The F^+-type centres in divalent compounds have *g*-shifts with both positive and negative signs; positive *g*-shifts were attributed to the participation in the ground state of configurations characterised as an F centre plus a hole on anions (Bartram *et al* 1967). In our case the unpaired spin may

also acquire hole characteristics by an increased participation of oxygen p functions in the Γ_1 ground state. Moreover, the increased admixtures of oxygen orbitals mean increased delocalisation and this gives a qualitative explanation for the appreciable reduction of the HF interaction constants of $(V_O)_2^{\cdot}$ compared to those of the $V_O^{\cdot}$ centre.

The strong non-axiality of A_c may be explained qualitatively by the fact that the –O–Te–O– chain in the model has two distinguished axes, the symmetry axis x and the chain direction z. Again, $A_z^{(c)} \gg A_y^{(c)}$ may be caused by strong admixtures of oxygen orbitals, but an appreciable d-type admixture on Te_c also seems to be involved. Apparently both types of admixtures are more pronounced for the divacancy centre.

In the LB-configuration model, however, where the core of the centre should be a strongly bent –O–Te–O– molecule in a plane perpendicular to z (bending angle 102° without relaxation), neither the outstanding g_z value nor the large $A_z^{(c)}$ value can be explained given the Γ_1 ground state in C_2, $\| x$ symmetry.

The extended character of the unpaired orbital along existing bonds emphasises the role of the outermost Te nuclei in the Te–O–Te_c–O–Te chain. Accordingly, this pair of nuclei has to be responsible for the SHF interaction with the largest constant A_I. The next SHF constant, A_{II}, may be related to Te nuclei on the other sides of the vacancies, since none of the weaker SHF interactions could be assigned to them in a straightforward way. Assignments for the Te shells III–XII are given in table 2 and partly in figure 7(*a*) and are based on a comparison of measured orientations of principal z axes of the SHF tensors with the Te_c–Te directions in the crystal. Although all deviations are less than 20°, these assignments remain tentative due to the appreciable covalency (shown by the dominating isotropic parts of the SHF interactions) and the non-monotonic $a(r)$ and $b(r)$ relations. Nevertheless the mapped area has an ellipsoid-like shape around Te_c with the orientation of the ellipsoid reflecting that of the centre core.

It is interesting to compare SHF interactions of the first few Te shells in the $(V_O)_2^{\cdot}$ and $V_O^{\cdot}$ centres (table 1). In fact a correspondence can be found corroborating the assignments for $(V_O)_2^{\cdot}$ and helping to propose new ones for the $V_O^{\cdot}$ centre (see figure 7(*b*)). The most important, nearly isotropic SHF interactions seem to correspond in both centres to Te ligands bound to LB oxygen neighbours of the central Te (A_I and the A_1, A_2 pair, respectively, indicated in table 1). To visualise Te partners I in $(V_O)_2^{\cdot}$ and 1, 2 in $V_O^{\cdot}$, see figure 7(*a*), (*b*). SHF constants for ligands assumed to be situated on the 'other side' of a vacancy or the remaining SB oxygen neighbour are grouped in the last column of table 1.

The trend from $V_O^{\cdot}$ to $(V_O)_2^{\cdot}$ then can be described as follows.

In the $V_O^{\cdot}$ centre the principal axis x of the $\mathbf{A}_s$ tensor (a characteristic direction of the wave-function) points towards a direction between [110] and the direction of the SB vacancy and makes an angle of only 15.3° with [110]. The appearance of the second SB vacancy tips the principal axis x of the HF (and $\mathbf{g}$) tensor to exactly [110] and at the same time causes stronger delocalisation of the spin along the LB directions, i.e. along the chain. This leads to reduced eigenvalues of $\mathbf{A}_c$, increases and equalises A_1 and A_2 to yield A_I, and decreases and equalises A_3 and A_4 to yield A_{II}. At the same time the appearence of a nearly degenerate ground state causes drastic changes in the g-values.

The $V_O^{\cdot}$ cluster model (Corradi *et al* 1987) was evidently too small to reflect correctly the SHF interactions, since the Te neighbours 1, 2 and 3 of figure 7(*b*) were only represented by terminating hydrogens, numbered 6, 5 and 4 in that model respectively. The new assignments of A_1–A_4 are still supported by the important spin populations on OH groups 6, 5 and 4 (i.e., on the respective hydrogens and their bridging oxygen partners) which are larger by nearly an order of magnitude than the spin population on

Te2 in that model (corresponding to the Te neighbour 4 of figure 7(*b*)). According to the new assignments for both $V_O^{\cdot}$ and $(V_O)_2^{\cdot}$ centres, the oxygen vacancies, compared to oxygen links, act more as a barrier for spin delocalisation, or, as suggested by the $V_O^{\cdot}$ cluster model, even as a barrier separating the unpaired spin and the surplus charge. A similar situation was reported for the E_1' centre in α-quartz by Yip and Fowler (1975).

An $S = \frac{1}{2}$ divacancy centre has been identified in irradiated silicon by Watkins and Corbett (1965) and was described by an extended orbital. However, no central nucleus was present and the wavefunction winding its way through vacancies (instead of atoms as in our case) resulted in g-values rather close to the free-spin value.

5.2. The peroxy radical

The most intense spectrum seen has a strong hole character ($\bar{g} = 2.111$), C_1 symmetry and two prominent Te splittings which are somewhat larger and much more anisotropic than those observed for the nearest ligands in the $V_O^{\cdot}$-type centres. These are clear indications for an unpaired spin mainly localised on oxygen orbitals but also having important densities on two adjacent telluriums. The centre core may comprise one or more oxygens.

The O^--type centres in various oxides including alkali earth oxides (V^--type centres; see, e.g., Kappers 1977), rutile structures (see, e.g., Bossoli *et al* 1979), Al_2O_3 (Bartram *et al* 1965, Du Varney *et al* 1985) and also less simple oxides, have a nearly free-spin g_z-value along the direction of the unpaired orbital and positive $\Delta g_{x,y}$-shifts smaller than 0.1. Our g-values in table 3 are rather different. Another argument against an O^- centre is the small probability of it having stabilising defects such as Te vacancies or appropriate impurities in large enough concentrations, which seems necessary to explain the high stability of the centre. O_2^{3-} defects can also be discarded due to their small g-shifts ($\Delta g \leqslant 0.03$); such defects are discussed by Requardt and Lehmann (1985).

O_2^- centres may have larger g-shifts ($g_z \gg g_e > g_{x,y}$), the largest g-value corresponding to the direction of the molecular axis and the smallest to the direction of the π-type hole state (Zeller and Känzig 1967). Apart from the somewhat large difference between g_x and g_y, the g-values observed in this work are quite similar to measured ones of O_2^- centres in most alkali halides (Zeller and Känzig 1967) and of a perturbed O_2^- defect in natural quartz with $g_x = 1.972$, $g_y = 1.959$ and $g_z = 2.318$ as observed by Baker and Robinson (1983).

In dry fused silica a peroxy radical was characterised which can be described as an asymmetric O_2^- ion substituted for the bridging oxygen in a Si–O–Si chain but bonded to only one Si (Friebele *et al* 1979). The semi-empirical cluster calculations of Edwards and Fowler (1982) confirmed this model showing that the association of the peroxy radical to only one Si and the breaking of the bond to the other Si happens only for large Si–Si separations in the chain, brought about by relaxation. They also predicted the existence of another more symmetric configuration of the peroxy radical which should be realised for smaller Si–Si distances (<3.8 Å). In this defect, which they called the small peroxy radical, one oxygen of the peroxy radical remained strongly bonded to both silicons. In TeO_2, where the smallest Te–Te distance is 3.74 Å and relaxations are expected to be small (Corradi *et al* 1987), a similar model could possibly explain the experimental data, including the nearly equally strong SHF interactions with the two Te's.

Such a configuration can in fact be constructed by adding an oxygen interstitial (O_i) to existing Te–O–Te chains in TeO_2 in such a way that the orientation of the peroxy

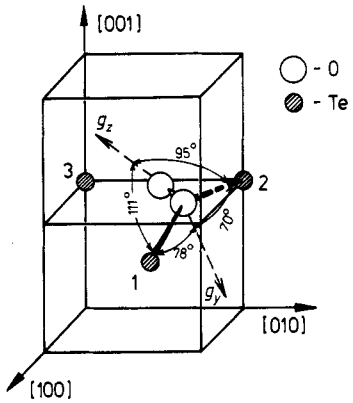

Figure 8. Model of the peroxy defect in TeO_2. The positions within the Te–O–Te chain correspond to perfect paratellurite with a bond angle of 140°. The SHF interactions characterised in table 3 are assigned to Te nuclei numbered 1, 2, and more tentatively, 3.

radical conforms both to the cited requirements of O_2^- theory and to the requirement of a nearly symmetric configuration with large Te–O–O_i angles, where this is needed for a reasonably isolated O_i end position in the peroxy radical. The choice of the configuration is unique and is shown in figure 8. The observed SHF interactions may be assigned to the Te nuclei numbered 1–3. The third Te is the next-nearest neighbour of O_i (the nearest neighbour of O_i is the other oxygen member of the radical). The Te(3)–O_i distance is 2.20 Å if a usual value of 1.30 Å is assumed for the internuclear distance in the peroxy radical. For this configuration the smallest g-value, g_y, in fact corresponds to the direction of an antibonding orbital that also forms large angles with Te–O bonds.

The large SHF constants of the two Te nuclei and the large difference g_x–g_y seem to be due to the rather covalent character of the Te–O bonds. An important delocalisation of the unpaired spin was also observed for the other intrinsic centres in TeO_2, in particular for $(V_O)_2^{\cdot}$. The spin densities on the Te nuclei can be estimated using results for the $V_O^{\cdot}$ centre where an isotropic HF constant of a = 1904 MHz corresponded to a calculated $\frac{2}{3}$ of the unpaired spin on Te_c (Corradi *et al* 1987). Accordingly, the isotropic parts of the SHF tensors assigned to Te nuclei 1 and 2, 525 and 439 MHz, respectively (see table 3) may correspond to 18 and 15% of the spin density, respectively. The anisotropic parts, which are of the same order of magnitude, indicate that important fractions of the densities come from Te p orbitals. An additional degree of freedom is the (unequal) distribution of the spin in the O_2^- group itself. A clear preference (~3 : 1) by the terminal oxygen for the spin, as obtained for the peroxy radical in SiO_2 by Friebele *et al* (1979), and supported for all cases considered by the results of Edwards and Fowler (1982), seems to be reasonable for explaining the observed g-values. In this case the wavefunction would simultaneously experience the axiality needed for a large Δg_z value and yet would have a strong enough inequivalence of the transverse directions for an appreciable difference between g_x and g_y.

Due to the present lack of a detailed calculation of the electronic structure only the following statements can be made. The peroxy model presented in figure 8 seems to account for all major features of the second new ESR spectrum. The intrinsic axial and inversion symmetry of the O_2^- molecule is strongly disturbed by the presence of (at least) two Te nuclei and this asymmetry is directly reflected in the non-axial character of the **g** tensor with the g_x direction roughly parallel to the line connecting both Te nuclei. The wavefunction is apparently less localised on the O_2^- group in TeO_2 than in SiO_2, where relatively weak SHF interaction with only one Si and smaller g_x–g_y differences have been

reported (Griscom and Friebele 1981, Baker and Robinson 1983). This parallels the similar difference between the $V_O^{\bullet}$ centre in TeO_2 and the E_1' centre in α-SiO_2 (see Watterich *et al* 1985).

Another question related to the covalency effects is that of the net charge of the defect. Two alternatives are considered, +1 and −1. The first corresponds to the ionic picture where the molecular ion O_2^- is thought to substitute for an O^{2-} ion. However, due to covalency the charge on the peroxy group may be more negative than that on a normal lattice oxygen. The latter was estimated by Corradi *et al* (1987) to be only $-\frac{1}{4}$ instead of the ionic −2. The charge on some tellurium ligands in the defect may also be more negative than for normal tellurium sites, which is a situation found for the central Te labelled s in the otherwise positively charged $V_O^{\bullet}$ centre (Corradi *et al* 1987). For reasons to be discussed in the next section, concerning defect production, we are inclined to accept a net negative charge for the peroxy defect.

5.3. Defect production in TeO_2

On the basis of the models of the three major stable paramagnetic intrinsic defects $V_O^{\bullet}$, $(V_O)_2^{\bullet}$ and the peroxy radical some conclusions concerning the processes in TeO_2 during electron irradiation can be drawn. The basic process may be a direct oxygen displacement (see, e.g., Meese and Locker 1972) leaving oxygen vacancy defects ($V_O^{\bullet}$-type defects) and O^- interstitials with the latter stabilised as peroxy centres near lattice oxygens. A similar process, but with neutral constituents of the Frenkel pair leading to diamagnetic defects, which would contribute only to optical absorption, cannot be excluded either. Oxygen vacancy defects may aggregate to form divacancies (such as the $(V_O)_2^{\bullet}$ centre) and associate with impurities. Therefore the $V_O^{\bullet}$ centre or a diamagnetic counterpart of this centre has to be mobile during RT electron irradiation. If the peroxy defect has a net negative charge as suggested in the previous section, neutrality of the crystal is provided for by approximately equal concentrations of the peroxy radical and the $V_O^{\bullet}$-type defects. This is in reasonable agreement with experiment.

6. Conclusions

In electron-irradiated α-TeO_2 we identified two further basic defects of the oxygen sublattice, the singly charged symmetric divacancy and an interstitial oxygen appearing as a substitutional peroxy radical. In both cases, even more than for the single-vacancy $V_O^{\bullet}$ centre, delocalisation of the unpaired spin along Te–O bonds has been observed, resulting in important superhyperfine interactions with ligands and strongly anisotropic **g** tensors. A comparison between the divacancy centre and the single vacancy centre showed that, in both cases, the unpaired spin is essentially concentrated on a quasi-linear Te–O–Te–O–Te chain situated next to the oxygen vacancy or vacancies.

Acknowledgments

The authors are grateful to Dr S Greulich-Weber and Mr Paul Generous for expert technical assistance. This work was supported by a joint project of the Deutsche Forschungsgemeinschaft (436 UNG-113) and the Hungarian Academy of Sciences, by the

US National Science Foundation under Grant No INT-8617352, the University of Connecticut Research Foundation and also by the National Scientific and Research Fund (OTKA) of Hungary.

References

Baker J M and Robinson P T 1983 *Solid State Commun.* **48** 551
Bartram R H, Swenberg C E and Fournier J T 1965 *Phys. Rev.* **139** A941
Bartram R H, Swenberg C E and La S Y 1967 *Phys. Rev.* **162** 759
Bossoli R B, Welsh T J, Gilliam O R and Stapelbroek M 1979 *Phys. Rev.* B **19** 4376
Corradi G, Bartram R H, Rossi A R and Janszky J 1987 *J. Phys. Chem. Solids* **48** 675
DuVarney R C, Niklas J R and Spaeth J-M 1985 *Phys. Status Solidi* b **128** 673
Edwards A H and Fowler W B 1982 *Phys. Rev.* B **26** 6649
Friebele E J, Griscom D L, Stapelbroek M and Weeks R A 1979 *Phys. Rev. Lett.* **42** 1346
Griscom D L and Friebele E J 1981 *Phys. Rev.* B **24** 4896
Kappers L A 1977 *Solid State Commun.* **21** 883
Kröger F A, Stieltjes F and Vink H J 1959 *Philips Res. Rep.* **14** 557
Lindquist O 1968 *Acta Chem. Scand.* **22** 977
Meese J M and Locker D R 1972 *Solid State Commun.* **11** 1547
Muenow D W, Hastie J W, Hauge R, Bautista R and Margrave J L 1969 *Trans. Faraday Soc.* **65** 3210
Niklas J R 1983 *Habilitationsschrift* Universität Paderborn
Requardt A and Lehmann G 1985 *J. Phys. Chem. Solids* **46** 107
Schmidt F and Voszka R 1981 *Cryst. Res. Technol.* **16** K127
Seidel H 1961 *Z. Physik* **165** 218, 239
Spaeth J-M 1988 *Exp. Tech. Phys.* **36** 257
Strömberg A, Wahlgreen U and Lindquist O 1985 *Chem. Phys.* **100** 229
Watkins G D and Corbett J W 1965 *Phys. Rev.* A **138** 543
Watterich A, Bartram R H, Gilliam O R, Kappers L A, Edwards G J, Voszka R and Cravero I 1986a *J. Phys. Chem. Solids* **47** 987
Watterich A, Bartram R H, Gilliam O R, Kappers L A, Edwards G J, Földvári I and Voszka R 1985 *Phys. Rev.* B **32** 2533
—— 1986b *Phys. Lett.* **117A** 247
Watterich A, Voszka R, Söthe H and Spaeth J-M 1987a *J. Phys. C: Solid State Phys.* **20** 3155
Watterich A, Bartram R H, Edwards G J, Gilliam O R, Földvári I and Voszka R 1987b *J. Phys. Chem. Solids* **48** 249
Yip K L and Fowler W B 1975 *Phys. Rev.* B **11** 2327
Zeller H R and Känzig W 1967 *Helv. Phys. Acta* **40** 845